University of Dayton
eCommons

Biology Faculty Publications

Department of Biology

6-2001

Salivary Acinar Cells from Aquaporin 5-deficient Mice Have Decreased Membrane Water Permeability and Altered Cell Volume Regulation

Carissa M. Krane
University of Dayton, ckrane1@udayton.edu

James E. Melvin
University of Rochester

Ha-Van Nguyen
University of Rochester

Linda Richardson
University of Rochester

Jennifer E. Towne
University of Cincinnati

See next page for additional authors

Follow this and additional works at: https://ecommons.udayton.edu/bio_fac_pub

🔵 Part of the Biology Commons, Biotechnology Commons, Cell Biology Commons, Genetics Commons, Microbiology Commons, and the Molecular Genetics Commons

eCommons Citation

Krane, Carissa M.; Melvin, James E.; Nguyen, Ha-Van; Richardson, Linda; Towne, Jennifer E.; Doetschman, Thomas; and Menon, Anil G., "Salivary Acinar Cells from Aquaporin 5-deficient Mice Have Decreased Membrane Water Permeability and Altered Cell Volume Regulation" (2001). *Biology Faculty Publications*. 131.
https://ecommons.udayton.edu/bio_fac_pub/131

Author(s)
Carissa M. Krane, James E. Melvin, Ha-Van Nguyen, Linda Richardson, Jennifer E. Towne, Thomas Doetschman, and Anil G. Menon

Salivary Acinar Cells from Aquaporin 5-deficient Mice Have Decreased Membrane Water Permeability and Altered Cell Volume Regulation*

Carissa M. Krane‡, James E. Melvin§, Ha-Van Nguyen§, Linda Richardson§, Jennifer E. Towne‡¶, Thomas Doetschman‡, and Anil G. Menon‡∥

From the ‡Department of Molecular Genetics, Biochemistry, and Microbiology, University of Cincinnati College of Medicine, Cincinnati, Ohio 45267-0524 and the §Center for Oral Biology, University of Rochester School of Medicine and Dentistry, Rochester, New York 14642

Aquaporins (AQPs) are channel proteins that regulate the movement of water through the plasma membrane of secretory and absorptive cells in response to osmotic gradients. In the salivary gland, AQP5 is the major aquaporin expressed on the apical membrane of acinar cells. Previous studies have shown that the volume of saliva secreted by AQP5-deficient mice is decreased, indicating a role for AQP5 in saliva secretion; however, the mechanism by which AQP5 regulates water transport in salivary acinar cells remains to be determined. Here we show that the decreased salivary flow rate and increased tonicity of the saliva secreted by $Aqp5^{-/-}$ mice in response to pilocarpine stimulation are not caused by changes in whole body fluid homeostasis, indicated by similar blood gas and electrolyte concentrations in urine and blood in wild-type and AQP5-deficient mice. In contrast, the water permeability in parotid and sublingual acinar cells isolated from $Aqp5^{-/-}$ mice is decreased significantly. Water permeability decreased by 65% in parotid and 77% in sublingual acinar cells from $Aqp5^{-/-}$ mice in response to hypertonicity-induced cell shrinkage and hypotonicity-induced cell swelling. These data show that AQP5 is the major pathway for regulating the water permeability in acinar cells, a critical property of the plasma membrane which determines the flow rate and ionic composition of secreted saliva.

The precise regulation of water and electrolyte transport in the acinar cells of the salivary gland is crucial for proper production of saliva. The fluid component of salivary secretions hydrates the oral cavity, aiding in the mastication and swallowing of food, in the neutralization of acids, and in protection against the invasion of potential pathogens. Clinically, salivary gland hypofunction commonly presents as xerostomia, a symptomatic complaint of dry mouth prevalent in the geriatric population (for review, see Ref. 1) which may result from either systemic or extrinsic causes (for review, see Refs. 1–3).

Saliva formation is a two-stage process (4, 5). First, the acinar cells secrete an isotonic plasma-like fluid, and second, ductal cells modify the acinar secretions primarily through the reabsorption of Na^+ and Cl^- so that the final saliva is hypotonic. This fluid secretion model predicts that saliva formation is primarily caused by transepithelial Cl^- transport and that Cl^- uptake is dependent on an inwardly directed Na^+ chemical gradient across the basolateral plasma membrane. An increase in intracellular Ca^{2+}, usually associated with muscarinic receptor stimulation, triggers fluid secretion by simultaneously activating apical Cl^- channels and basolateral K^+ channels. The efflux of Cl^- and K^+ across the apical and basolateral membranes, respectively, produces a transepithelial potential difference that is neutralized by paracellular Na^+ transport across tight junctions. The resulting transepithelial osmotic gradient drives the movement of water, creating a plasma-like primary secretion.

In salivary gland acinar cells, secretion is associated with cell volume changes (6, 7). The shrinkage and swelling of salivary gland acinar cells following muscarinic and β-adrenergic stimulation, respectively, are thought to occur as a result of an imbalance between the influx and efflux of ions (specifically Cl^-) between the luminal and basolateral membranes (8). The resulting change in tonicity requires a rapid and regulated change in acinar cell water permeability which is necessary for secretion and maintenance of cell volume following stimulation.

Aquaporin 5 (AQP5),[1] a mercury-sensitive water channel, has been localized to the luminal surface of acinar cells in the salivary gland, the site of salivary secretion (9). Recently Ma *et al.* (10) showed that AQP5-deficient mice secrete a low volume of viscous hypertonic saliva after supramaximal pilocarpine stimulation. They hypothesized that AQP5 plays a role in regulating membrane water permeability and that it is also required for maintaining proper osmolality of the secreted saliva, although a mechanism by which this is accomplished was not examined. The results of this study are consistent with at least two potential mechanisms whereby hyposalivation might be induced in mice lacking AQP5. The simplest explanation is that AQP5 acts as the apical water pathway during stimulated fluid

[1] The abbreviations used are: AQP5, aquaporin 5; kb, kilobase(s); bp, base pair(s); ES cell(s), embryonic stem cell(s); RVD, respiratory volume decrease; PGK, phosphoglycerate kinase.
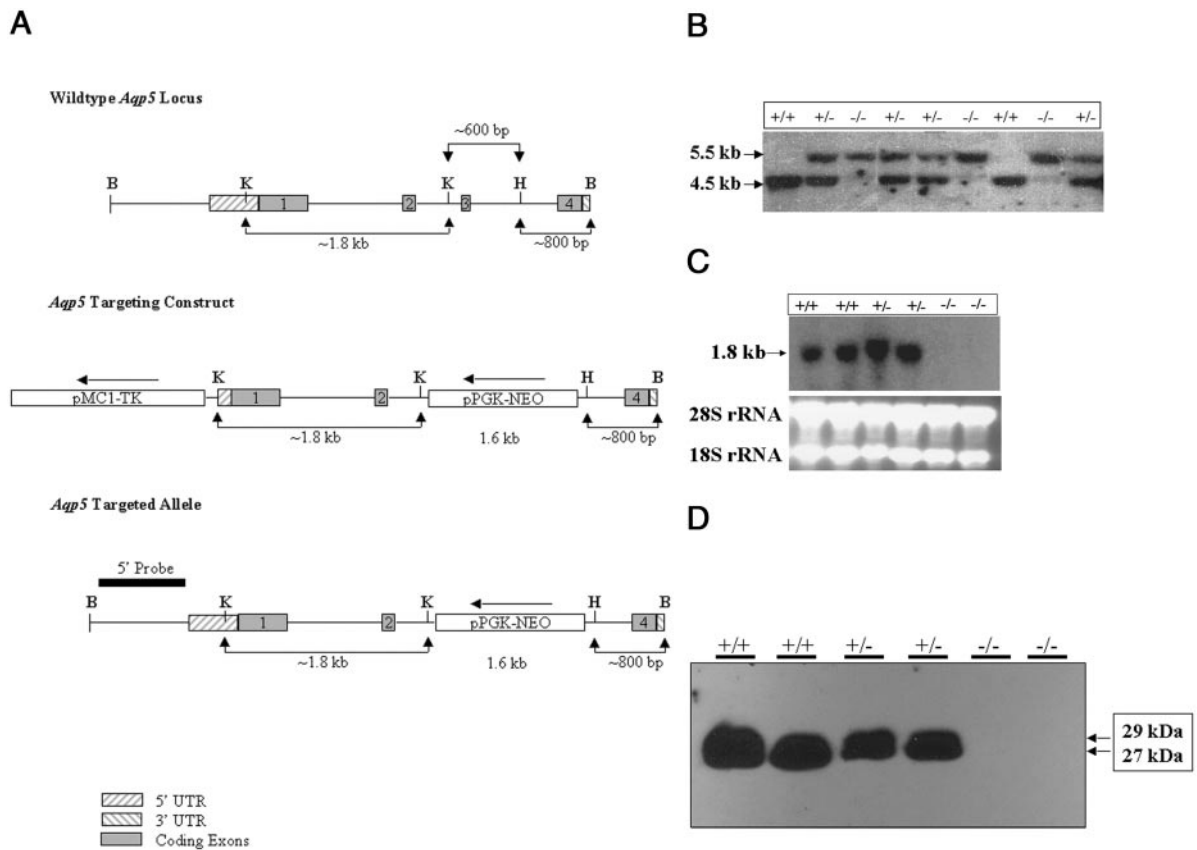
FIG. 1. **Mouse *Aqp5* gene targeting construct, Southern, Northern, and Western analyses.** *Panel A*, generation of an *Aqp5* locus-specific replacement type targeting vector. A schematic of the genomic organization and partial restriction map of the wild-type mouse *Aqp5* locus based on analysis of a 129SvJ genomic subclone (11) is shown. *B*, *Bam*HI; *H*, *Hin*dIII; *K*, *Kpn*I. Exons are shown as indicated. Two fragments of the *Aqp5* locus, a 1.8-kb *Kpn*I left arm fragment and a 0.8-kb *Hin*dIII/*Bam*HI right arm fragment, were inserted to flank the 3′- and 5′-ends of the PGK-neomycin resistance cassette (pPGK-NEO), respectively. A herpes simplex virus-thymidine kinase expression cassette (pMC1-TK) was positioned outside of the homologous segment, 5′ of the left arm in the 3′-5′ orientation. The replacement construct deletes 55 bp of intron 2, the entire exon 3 (84 bp), and 467 bp of intron three and replaces them with a 1.6-kb PGK-neomycin minigene cassette, resulting in a net addition of 1 kb. A 931-bp 5′-screening probe outside of the homologous region is indicated. *UTR*, untranslated region. *Panel B*, genotypic analysis of an F2 litter from sibling matings of *Aqp5* heterozygous F1 founders. Mouse tail DNA was isolated and digested with *Bam*HI. Southern hybridization was performed using a 931-bp 5′-screening probe. All three genotypes are represented in this litter: +/+ (4.5 kb), +/− (4.5 kb/5.5 kb), and −/− (5.5 kb). *Panel C*, Northern hybridization of total RNA from *Aqp5⁺/⁺*, *Aqp5⁺/⁻*, and *Aqp5⁻/⁻* parotid glands. A mouse AQP5 cDNA clone containing the entire open reading frame and 3′-untranslated region was α-^{32}P labeled and used to hybridize 20 μg of adult mouse parotid gland total RNA from *Aqp5⁺/⁺*, *Aqp5⁺/⁻*, and *Aqp5⁻/⁻* mice (*n* = 2 each genotype). A 1.8-kb transcript is indicated with an *arrow*. The 28 S and 18 S rRNA bands were visualized by UV illumination of the ethidium bromide-stained agarose gel and are shown to demonstrate RNA quality and loading. *Panel D*, Western analysis of total membrane preparations from *Aqp5⁺/⁺*, *Aqp5⁺/⁻*, and *Aqp5⁻/⁻* parotid glands. An AQP5 rabbit polyclonal antibody (LL639; 0.5 μg/ml) generated against a C-terminal peptide specific to mouse AQP5 sequence was used in immunoblotting experiments against 20 μg of total membrane proteins isolated from the parotid glands of *Aqp5⁺/⁺*, *Aqp5⁺/⁻*, and *Aqp5⁻/⁻* mice. Two immunoreactive bands at 27 and 29 kDa are indicated in the *Aqp5⁺/⁺* and *Aqp5⁺/⁻ lanes* by *arrows* but are absent in the *Aqp5⁻/⁻ lanes* (*n* = 2 each genotype). Protein isolation and Western blotting were performed as described (see "Experimental Procedures").

secretion, although no basolateral channel has been identified as yet. Alternatively, targeted disruption of the *Aqp5* gene may alter whole animal water balance, resulting in an increase in the osmolarity of the blood. Previous studies clearly show that dehydration increases the osmolarity of blood, and this in turn correlates with decreased salivation (11, 12)

Here we directly measure membrane water permeability of isolated acinar cells from *Aqp5⁺/⁺* and *Aqp5⁻/⁻* mice as well as flow rates and osmolality measurements of secreted saliva. Hyposalivation is not caused by changes in whole body fluid homeostasis, but instead, we demonstrate that the membrane permeability of salivary gland acinar cells is dramatically reduced in mice lacking AQP5. Our results are the first to provide a mechanism for AQP5 function during salivary secretion.

EXPERIMENTAL PROCEDURES

Generation of Aqp5 Replacement Targeting Construct—Mouse genomic clones containing the *Aqp5* locus were isolated from a 129SvJ DNA bacteriophage λ library by hybridization with an AQP5 partial cDNA clone and characterized as described (13). Two fragments of the *Aqp5* locus, an ~1.8-kb *Kpn*I fragment extending from within exon 1

through intron 2, and an ~800-bp *Hin*dIII/*Bam*HI fragment extending from intron 3 to within the 3′-untranslated region of exon 4, were inserted to flank the 3′- and 5′-ends of a PGK-neomycin resistance gene (14), respectively. A herpes simplex virus-thymidine kinase expression cassette (pMC1-TK (14)) was placed outside of the homologous segments, 5′ to the left arm, to provide selection against random insertion of the targeting vector.

Embryonic Stem Cell Targeting—Isogenic ES cells derived from the 129SvJ mouse strain were electroporated with 50 μg of linearized targeting vector. After electroporation, the cells were subjected to selection with G418 and gancyclovir as described (15). A 931-bp diagnostic probe 5′ to the homologous region represented in the targeting vector was used to screen 187 ES cell clones by Southern analysis. The probe was polymerase chain reaction amplified from an AQP5 genomic clone (13) using 10 pmol of each primer (forward primer (4.5 Seq) 5′-CCG-GCAGAAACAAAGACCT-3′; reverse primer (Pri Ext 3) 5′-CGCATCGT-GCGCTCAGCG-3′); 0.25 mM each dNTP, 2.0 mM MgCl$_2$, 60 mM Tris-HCl at pH 9.0, 12.5 mM (NH$_4$)$_2$ SO$_4$, 10 ng of 2.1/4.5 plasmid DNA (11), 0.1 unit of *Taq* polymerase (Life Technologies, Inc.) in a total reaction volume of 20 μl. Polymerase chain reaction was performed in an MJ PTC-100 Thermocycler device (Watertown, MA) with the following conditions: 94 °C for 2 min; (92 °C for 30 s −57 °C for 1 min −72 °C for 1 min) 35 times; −72 °C for 7 min. Products were separated by gel
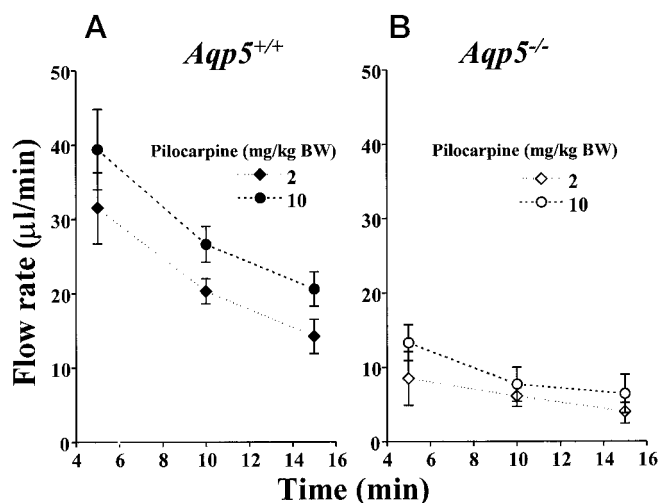
FIG. 2. **Severe impairment of salivation in Aqp5$^{-/-}$ mice.** Saliva flow rates for Aqp5$^{+/+}$ (*panel A*) and Aqp5$^{-/-}$ (*panel B*) mice ($n = 6$ each genotype) were determined over three 5-min intervals (5, 10, and 15 min) after intraperitoneal administration of two physiological doses of the sialagogue pilocarpine HCl (2 or 10 mg/kg of body weight).

TABLE I
Osmolality of pilocarpine-stimulated salivary secretion
Statistically significant values are indicated (*) ($p < 0.05$).

Agonist concentration	Osmolality	
	Aqp5$^{+/+}$	Aqp5$^{-/-}$
2 mg pilocarpine/kg body weight		
5 min	165.8 ± 6.5	225.8 ± 16.6*
10 min	174.0 ± 11.1	229.7 ± 18.4*
15 min	173.0 ± 10.7	246.8 ± 17.0*
10 mg pilocarpine/kg body weight		
5 min	196.5 ± 4.1	257.0 ± 9.8*
10 min	216.5 ± 10.1	271.8 ± 14.6*
15 min	221.5 ± 6.9	272.3 ± 10.1*

electrophoresis on a 1% low melting point agarose (Life Technologies, Inc.) in 1 × TAE buffer and gel extracted (Qiagen gel extraction kit, Valencia, CA). The replacement construct deletes 55 bp of intron 2, the entire exon 3 (84 bp), and 467 bp of intron 3, and replaces them with the 1.6-kb PGK-neomycin cassette. ES cell lines with a correctly targeted *Aqp5* allele resulting from homologous recombination were identified by the presence of a neomycin-containing (5.5 kb) and wild-type (4.5 kb) *Bam*HI fragment.

Generation of Aqp5-deficient Mice—Two ES cell clones (175 and 187) were used in blastocyst-mediated transgenesis (16). 11 mice, 30–90% chimeric for the ES cell-derived 129SvJ agouti coat color, were generated. Germline transmission of the targeted allele was obtained from five chimeric male matings to outbred Black Swiss females. Those offspring carrying 129SvJ-derived genetic material were identified by their agouti coat color, and those carrying the targeted allele were determined by Southern analysis of tail DNA using the diagnostic probe described above. Intercross sibling matings of the F1 animals heterozygous for the targeted allele were used to establish recombinant inbred 129SvJ × Black-Swiss *Aqp5* targeted lines. Mice used throughout this study were *Aqp5$^{+/+}$*, *Aqp5$^{+/-}$*, and *Aqp5$^{-/-}$* age- and sex-matched littermates from the F3 generation of recombinant inbred *Aqp5* targeted 129SvJ × Black Swiss genetic background.

Histology—Gross histological analysis was performed by Dr. Greg Boivin (Department of Comparative Pathology, University of Cincinnati College of Medicine) on submandibular, sublingual, and parotid glands from *Aqp5$^{+/+}$*, *Aqp5$^{+/-}$*, and *Aqp5$^{-/-}$* age- and sex-matched littermates by light microscopic analysis of paraformaldehyde-fixed paraffin-embedded hematoxylin and eosin-stained tissue sections (not shown).

Northern Analysis—Total RNA was prepared from submandibular, sublingual, and parotid glands dissected from adult *Aqp5$^{+/+}$*, *Aqp5$^{+/-}$*, and *Aqp5$^{-/-}$* littermates and analyzed by Northern blot with an AQP5 cDNA clone as described (13). Equal loading and quality of RNA samples were confirmed by the relative abundance of the 28 S and 18 S rRNA bands visualized by UV illumination of the ethidium bromide-stained gel.

Western Analysis—Total membrane preparations from submandibular, sublingual, and parotid glands were isolated from adult *Aqp5$^{+/+}$*, *Aqp5$^{+/-}$*, and *Aqp5$^{-/-}$* littermates and analyzed by immunoblotting with 0.5 µg/ml rabbit polyclonal anti-AQP5 peptide derived antibody (LL639) as described (13). Equal loading of membrane samples was confirmed by Coomassie Blue staining of SDS-polyacrylamide gels.

Cell Volume Determinations—Parotid and sublingual acini from adult (8–20 weeks old) *Aqp5$^{+/+}$* and *Aqp5$^{-/-}$* age- and sex-matched littermates were dispersed as described previously (17). Briefly, mice were killed by exsanguination after exposure to CO_2 gas. The parotid and sublingual glands were quickly removed, trimmed of connective tissues, and minced finely in digestion medium (Eagle's modified essential medium, Biofluids, Inc., Rockville, MD) containing collagenase P (0.3 mg/7.5 ml/animal) + 1% bovine serum albumin. The minced glands were incubated at 37 °C in a shaker with continuous agitation (100

cycles/min). After the first 20-min interval the minced glands were dispersed by gentle pipetting (10 times) with a 10-ml plastic pipette and centrifuged (210 × *g* for 15 s). The supernatant was discarded, and the pellet was resuspended in 7.5 ml of collagenase digestion medium for an additional 40 min, and the acinar cells were then rinsed and harvested by centrifugation. The dispersed acinar cells were loaded with the fluoroprobe calcein by incubation for 15 min at room temperature in 2 µM calcein-AM (Molecular Probes, Eugene, OR).

Cell volume was estimated by confocal microscopy, as described (18). Cells were allowed to adhere to the base of a superfusion chamber mounted on an Olympus PMT2 fluorescence microscope interfaced with an Ultima™ confocal microscope (Genomic Solutions, Ann Arbor, MI). Intracellular dye was excited with 488 nm band of an argon laser and emitted fluorescence measured at 530 nm. Changes in cell volume were monitored by measuring the fluorescence intensity of calcein within a defined intracellular volume. In combination with an Olympus DplanApo 40× objective, a 225-µm confocal pinhole produces an ~4-µm-thick optical section in the *z* direction. Using Ultima™ software, an *x-y* area of the two-dimensional image was circumscribed within individual acini. In some experiments, cell volume was estimated using a Nikon Diaphot 200 microscope interfaced with an Axon Imaging Workbench system (Foster City, CA). Cells were excited at 490 nm, and emitted fluorescence was measured at 530 nm. The initial linear rate of cell volume change was used as an index of acinar cell water permeability. Cell volume was correlated with fluorescence by *in situ* calibration of the dye performed using solutions of different osmolalities. The relationship between dye fluorescence and the volume change was linear over a volume range from +30% to −30%, which is within the physiological range of cell volume changes observed in acinar cells. Cell volume was expressed in arbitrary units as 1/normalized calcein fluorescence.

Mercury-sensitive Water Permeability—The initial linear rate of cell volume change was used as an index of acinar cell water permeability. *Aqp5$^{+/+}$* and *Aqp5$^{-/-}$* parotid and sublingual acinar cells were enzymatically dispersed and loaded with fluorescent dye as described above and subsequently equilibrated in an isosmotic (~300 mosM), intracellular-like solution to eliminate ion gradients. The solution contained 15 mM NaCl, 50 mM KCl, 75 mM potassium gluconate, 0.4 mM KH_2PO_4, 0.33 mM NaH_2PO_4, 20 mM Hepes, 10 mM glucose, 0.8 mM $MgSO_4$, and 1.2 mM $CaCl_2$. A 30% hyperosmotic shock was induced by perfusion of acini in the above solution containing 90 mM sucrose, and the rate of cell volume change was determined ("control" rate). Sucrose was then removed to permit the cell volume to reequilibrate before exposure to 1 mM $HgCl_2$ for 5 min. The same cells were then exposed to a second hypertonic shock in the presence of $HgCl_2$. The rate of volume change in the presence of 1 mM $HgCl_2$ was used to calculate the mercury-sensitive water permeability of acinar cells.

Hyposmotic Shock and the Associated Regulatory Volume Decrease (RVD)—*Aqp5$^{+/+}$* and *Aqp5$^{-/-}$* parotid and sublingual acinar cells were enzymatically dispersed and loaded with fluorescent dye as above, and then equilibrated in an isosmotic physiological solution containing 135 mM NaCl, 5.4 mM KCl, 0.4 mM KH_2PO_4, 0.33 mM NaH_2PO_4, 20 mM Hepes, 10 mM glucose, 0.8 mM $MgSO_4$, and 1.2 mM $CaCl_2$. Hyp_osmotic cell swelling was induced by switching the perfusate to the above solution after diluting by 30% with water. Cell volume change was measured as described above by monitoring the change in calcein fluorescence. The rate of RVD was determined over the course of ~300 s while the cells remained in the hyposmotic solution.

Stimulated Flow Rates and Saliva Composition—Adult *Aqp5$^{+/+}$* and *Aqp5$^{-/-}$* age- and sex-matched littermates (12–16 weeks of age, $n = 6$

TABLE II

Water intake, urine output, urine osmolality and electrolytes

Values are expressed as the mean ± S.E.

	Water intake		Urine output		Urine osmolality (n = 12)	Urine electrolytes		
	Male (n = 6)	Female (n = 6)	Male (n = 6)	Female (n = 6)		Na$^+$	K$^+$	Cl$^-$
	ml/g body weight ± S.E.		*ml/g body weight ± S.E.*		*mosm/kg H$_2$O*	*meq/liter*		
Wild-type	0.151 ± 0.013	0.136 ± 0.019	0.074 ± 0.012	0.046 ± 0.007	2824 ± 206	427.6 ± 43.1	298.0 ± 25.1	368.6 ± 20.3
Knockout	0.124 ± 0.020	0.135 ± 0.012	0.055 ± 0.07	0.035 ± 0.008	3149 ± 244.9	459.4 ± 43.7	333.0 ± 25.5	417.2 ± 24.1

TABLE III

Blood gas and plasma electrolyte measurements of Aqp5$^{+/+}$ and Aqp5$^{-/-}$ mice

Values are the means ± S.E.

	Blood gas/electrolyte						
	pH	pCO$_2$	pO$_2$	Na$^+$	K$^+$	Cl$^-$	HCO$_3^-$
		mm Hg			*meq/liter*		
Aqp5$^{+/+}$	7.436 ± 0.011	31.950 ± 1.994	83.833 ± 5.703	149.333 ± 0.422	5.945 ± 0.252	113.000 ± 0.856	21.240 ± 0.823
Aqp5$^{-/-}$	7.437 ± 0.015	35.160 ± 0.829	82.460 ± 3.795	150.8 ± 0.583	5.968 ± 0.288	113.000 ± 0.837	22.775 ± 0.641

each group) were anesthetized with an intraperitoneal injection of 300 mg of chloral hydrate/kg of body weight and then stimulated with either 2 or 10 mg of pilocarpine HCl/kg of body weight (BW). Whole saliva was collected, representing a combination of parotid, submandibular, and sublingual secretions, with a very minor component from minor salivary, nasal, and tracheal glands. Saliva was collected from the lower cheek pouch by a suction device at intervals of 5, 10, and 15 min and expressed as μl/min. The osmolality of the saliva was measured using a vapor pressure osmometer (Wescor 5500, Logan, UT).

Water Intake and Urine Output Analysis—Adult Aqp5$^{+/+}$ and Aqp5$^{-/-}$ littermates (n = 12 each genotype; n = 6 male, n = 6 female per genotype) were housed one per metabolic cage and acclimated for 48 h prior to urine collection. Mice had free access to drinking water and standard 1% NaCl mouse chow diet throughout the experiment. Baseline urine samples were collected over a period of 24 h for 3 consecutive days, and the volume, electrolyte composition, and osmolality were recorded. Aliquots of urine samples were centrifuged at 10,000 × g for 5 min to remove any suspended material, and the supernatants were used to measure the osmolality by freezing point depression on a Fiske One-Ten Osmometer (Norwood, MA). Sodium and potassium concentrations (meq/liter) were determined using a Ciba-Corning Flame photometer, model 480 (Medfield, MA), and chloride (meq/liter) was determined using a Labconco Digital Chloridometer (Kansas City, MO). The volume of water intake/24 h was recorded. Body weight was recorded prior to acclimation and at every 24-h time point. The mean average of 3 days of collection was calculated for each parameter measured, normalized for body weight, and used in statistical analysis comparing sex-matched wild-type *versus* knockout mice.

Blood Gas and Electrolyte Analysis—Tail vein blood (50 μl) was collected from adult Aqp5$^{+/+}$ and Aqp5$^{-/-}$ age- and sex-matched littermates (12–16 weeks of age, n = 6 each genotype) and analyzed for gases, electrolytes, and pH as described (19).

Statistical Analyses—All cell volume measurements were expressed in arbitrary units as 1/normalized calcein fluorescence for the indicated number of acini studied (n). Experiments were repeated using at least three separate preparations. Data were analyzed by a two-tailed Student's t test, and differences between test and control values at $p < 0.05$ were considered to be statistically significant.

RESULTS

Generation of Aqp5$^{-/-}$ Mice—The Aqp5 targeted allele was generated by replacing 600 bp of the mouse Aqp5 gene, which includes a portion of intron 2, all of exon 3, and a portion of intron 3, with the neomycin resistance gene (Fig. 1A). The targeted replacement results in the deletion of extracellular loop E of the mouse AQP5 protein, which contains the highly conserved Asn-Pro-Ala (NPA) motif (20) and the mercury-sensitive cysteine residue at position 182 (13). Alterations in the NPA motifs in either the B or E loops have been shown to disrupt water permeability in aquaporin family members (21). Six independently derived Aqp5 targeted ES cell lines were identified by the presence of both 5.5-kb and 4.5-kb BamHI fragments by Southern analysis corresponding to the targeted

and wild-type alleles respectively (not shown). Chimeras were generated through blastocyst injection of two ES cell lines, and germline transmission was obtained. A representative Southern blot from an F1 heterozygous mating is shown in Fig. 1B. We observed a birth genotypic ratio of 1 (+/+): 2 (+/−): 0.5 (−/−), suggesting a role for Aqp5 in prenatal survival. Adult Aqp5$^{-/-}$ mice weighed ~90% of their Aqp5$^{+/+}$ and Aqp5$^{+/-}$ age- and sex-matched littermates (not shown). No difference in morbidity, mortality, or longevity was observed among the three genotypes from birth to >1 year of age (not shown). Submandibular, sublingual, and parotid glands from 12–16-week-old Aqp5$^{+/+}$, Aqp5$^{+/-}$, and Aqp5$^{-/-}$ littermates were histologically normal as revealed by light microscopic analysis of hematoxylin and eosin-stained tissue sections (not shown).

Northern Analysis of Salivary Gland Total RNA—Northern analysis was performed on total RNA isolated from parotid glands from Aqp5$^{+/+}$, Aqp5$^{+/-}$, and Aqp5$^{-/-}$ littermates using a mouse AQP5 cDNA probe containing the entire open reading frame and the 3′-untranslated region. A 1.8-kb band corresponding to the mouse AQP5 transcript was observed in RNA from +/+ and +/− mice but was not present in the RNA from Aqp5$^{-/-}$ glands (Fig. 1C). Thus, the targeted replacement of the Aqp5 locus results in the absence of AQP5 mRNA in Aqp5$^{-/-}$ mouse salivary glands. Identical results were obtained with total RNA from the sublingual and submandibular glands (not shown).

Western Analysis of Salivary Gland Total Membrane Preparations—Immunoblotting of total membrane fractions prepared from parotid glands from Aqp5$^{+/+}$, Aqp5$^{+/-}$, and Aqp5$^{-/-}$ mice with an anti-AQP5 peptide-derived rabbit polyclonal antibody identified both the 27-kDa and 29-kDa AQP5 immunoreactive bands in Aqp5$^{+/+}$ and Aqp5$^{+/-}$ mice, which were reported previously in mouse salivary glands (13). Neither the 27-kDa nor the 29-kDa bands were present in Aqp5$^{-/-}$ membrane fractions (Fig. 1D). Therefore, the targeted replacement of the Aqp5 locus ablates AQP5 protein production and results in AQP5 null mice. Identical results were obtained with total membrane fractions from the sublingual and submandibular glands (not shown).

Salivary Flow Rate—A previous study has shown that Aqp5-deficient salivary glands produce less saliva in response to a supramaximal concentration of a cholinergic agonist (80 mg/kg pilocarpine), and the saliva was hypertonic (420 mosm) (10) rather than hypotonic as in wild-type mice. In the present study, two different physiological concentrations of agonist (2 and 10 mg of pilocarpine HCl/kg of body weight, injected intraperitoneally) were used to stimulate salivary secretion. The
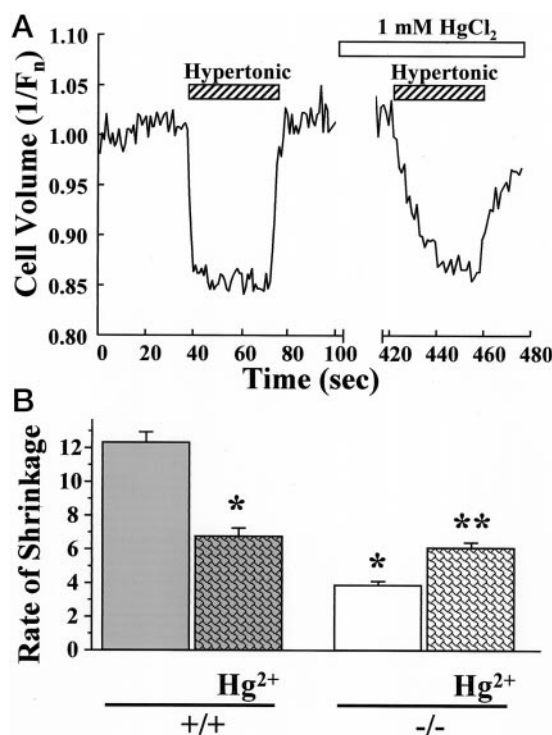
FIG. 3. **Cell volume changes: mercury-sensitive hypertonicity-induced parotid acinar cell shrinkage.** *Panel A*, hypertonicity-induced rate of shrinkage of parotid acinar cell from wild-type mice and the effect of HgCl$_2$. HgCl$_2$ inhibits the rate of *Aqp5$^{+/+}$* parotid acinar cell volume changes induced by hypertonic shock. The cell volume of mouse parotid acinar cells was estimated by confocal microscopy using the intracellular fluorescent dye calcein. Acinar cells were loaded with the fluoroprobe by incubation for 15 min with 2 μM calcein-AM, and the fluorescence intensity emitted from within a defined intracellular volume was monitored. The normalized fluorescence intensity (F_n) increases as cell volume decreases in response to hypertonic shock. Parotid acinar cells from wild-type mice were exposed to a hypertonic shock by the addition of 60 mM sucrose during the time indicated by the *cross-hatched rectangle* to determine the control rate of water permeability. Cells were then returned to an isosmotic solution and treated with 1 mM HgCl$_2$ for 5 min (indicated by the *open rectangle*; note the break in the *x* axis) followed by exposure to a second hypertonic shock in the continued presence of HgCl$_2$. Changes in cell volume are expressed as 1/F_n. *Panel B*, summaries of the rates of hypertonicity-induced *Aqp5$^{+/+}$* and *Aqp5$^{-/-}$* parotid acinar cell shrinkage in the absence and presence (*stippled bar*) of 1 mM HgCl$_2$. The *asterisks* (*) indicate a significant difference in the rate of cell shrinkage of *Aqp5$^{+/+}$* (*filled bar*) in the presence of mercury (~50%; $p < 0.0001$, $n \geq 36$), and a ~65% decrease in *Aqp5$^{-/-}$* (*open bar*) compared with the intrinsic *Aqp5$^{+/+}$* rate. The membrane permeability of *Aqp5$^{-/-}$* acinar cells was enhanced (** $p < 0.0001$; $n \geq 36$) in the presence of mercury compared with untreated *Aqp5$^{-/-}$* cells.

pilocarpine-stimulated salivary flow rate was determined for *Aqp5$^{+/+}$* and *Aqp5$^{-/-}$* mice at three 5-min intervals over the course of 15 min (see Fig. 2). The flow rate for *Aqp5$^{-/-}$* mice at all three intervals with both pilocarpine concentrations was inhibited significantly compared with the rate observed for *Aqp5$^{+/+}$* mice (range = 45–80% of the control rate; mean ± S.E. = 64.7 ± 6.8% inhibition). Thus, AQP5 deficiency results in a sustained ~65% decrease in the rate of pilocarpine-stimulated saliva flow regardless of the agonist concentration used. These data demonstrate that AQP5 is critically important to salivation, independent of the magnitude of receptor activation.

Salivary Osmolality—In addition to flow rate measurements, the osmolality of stimulated salivary secretions was determined for three 5-min intervals over a 15-min duration after stimulation with 2 or 10 mg of pilocarpine/kg of body weight (Table I). Osmolality was increased significantly ($p <$
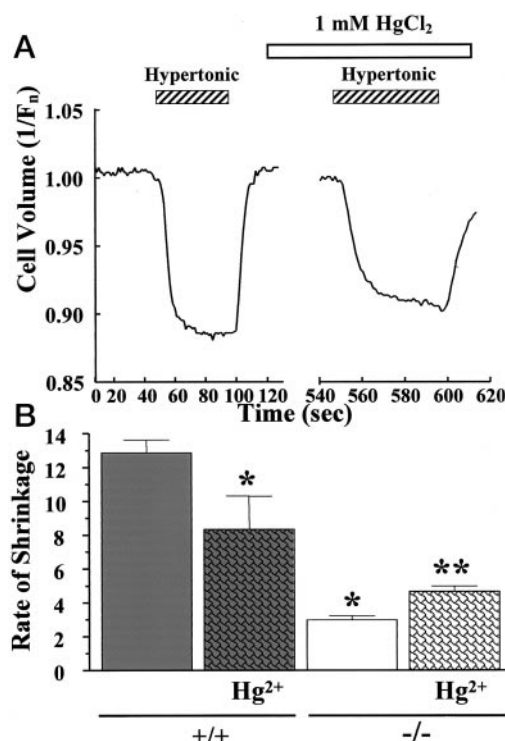

FIG. 4. **Cell volume changes: mercury-sensitive hypertonicity-induced sublingual acinar cell shrinkage.** *Panel A*, HgCl$_2$ inhibits sublingual acinar cell volume changes induced by hypertonic shock (for description of the protocol, see the Fig. 2A legend). *Panel B*, summaries of the rates of hypertonicity-induced *Aqp5$^{+/+}$* and *Aqp5$^{-/-}$* sublingual acinar cell shrinkage in the absence and presence (*stippled bar*) of 1 mM HgCl$_2$. The *asterisks* (*) indicate a significant decrease in the rate of hypertonicity-induced cell shrinkage of *Aqp5$^{+/+}$* (*filled bar*) in the presence of mercury (~35%; $p < 0.0001$, $n \geq 36$) and a ~77% decrease in *Aqp5$^{-/-}$* (*open bar*) compared with the intrinsic *Aqp5$^{+/+}$* rate. The membrane permeability of *Aqp5$^{-/-}$* acinar cells was enhanced (** $p < 0.0001$; $n \geq 36$) in the presence of mercury compared with untreated *Aqp5$^{-/-}$* cells.

0.01) in the saliva from *Aqp5$^{-/-}$* mice compared with their wild-type littermates, and it remained increased over the collection period at all three intervals (Table I). These results indicate that the final osmotic composition of stimulated saliva is affected by AQP5 expression.

Fluid Intake and Urine Output—To determine whether the absence of AQP5 affects whole animal fluid homeostasis, water intake and urinary volume output were monitored in adult *Aqp5$^{+/+}$* and *Aqp5$^{-/-}$* mice (Table II). Interestingly, there were no significant differences in the volume of water intake or urine excreted by *Aqp5$^{-/-}$* mice compared with their age- and sex-matched littermates. In addition, urine osmolality, potassium, sodium, and chloride concentrations did not differ between wild-type and AQP5 knockout mice (Table II).

Blood Gas and Electrolyte Analysis—To examine the role of AQP5 in the maintenance of blood gas and plasma electrolyte homeostasis, blood samples from awake adult *Aqp5$^{+/+}$* and *Aqp5$^{-/-}$* mice were collected and analyzed for plasma electrolytes, blood pH, and blood gas levels. No significant differences were observed in these parameters when comparing the AQP5 knockout mice with wild-type littermates (Table III). Taken together, the results shown in Tables II and III demonstrate that the hyposalivation observed in *Aqp5$^{-/-}$* mice is *not* caused by changes in whole animal fluid and electrolyte homeostasis.
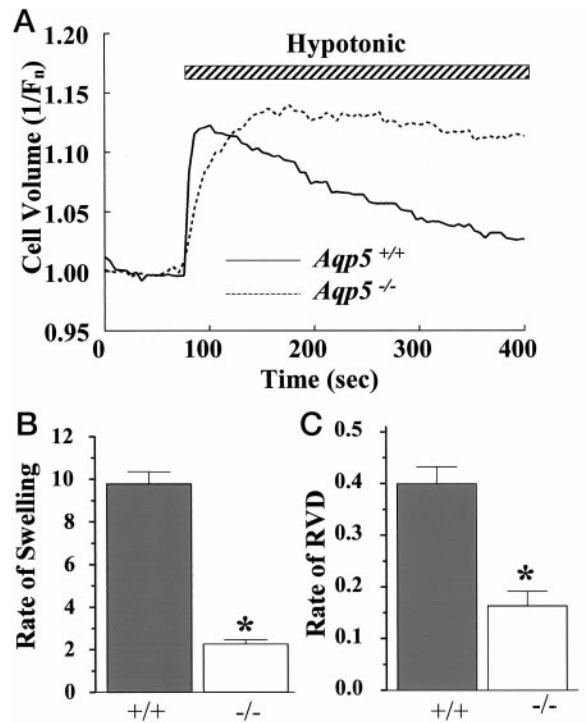
AQP5-dependent and Mercury-sensitive Acinar Cell Water Permeability—AQP5 was initially identified and cloned from the rat submandibular gland and was shown to be a mercury-sensitive water channel (22). To examine whether AQP5 is

Salivary Gland Hypofunction in Aqp5$^{-/-}$ Mice
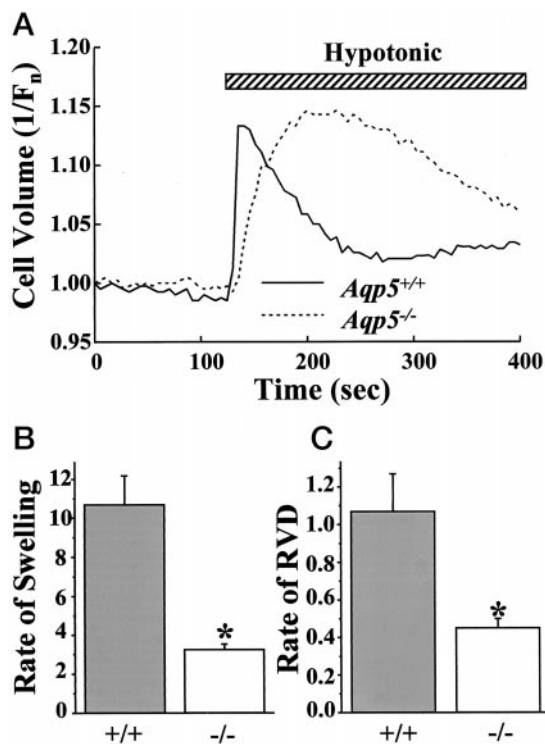
FIG. 5. **Targeted disruption of the *Aqp5* gene inhibits the hypotonicity-induced cell swelling and the associated RVD in parotid acinar cells.** The role of AQP5 in the RVD response was examined in parotid acinar cells loaded with calcein as described under "Experimental Procedures." *Panel A*, parotid acini isolated from *Aqp5$^{+/+}$* (*solid line*) and *Aqp5$^{-/-}$* (*dotted line*) were perfused in an isosmotic solution, and then hyposomotic cell swelling was induced by switching the perfusate to a second medium diluted with 30% water during the time interval indicated by the *cross-hatched rectangle*. Changes in cell volume are represented as values of 1/F_n. *Panels B and C*, summaries of the relative rates of swelling (*panel B*) and RVD (*panel C*), respectively, in *Aqp5$^{+/+}$* (*filled bar*) and *Aqp5$^{-/-}$* (*open bar*) of parotid acinar cells. Values represent mean ± S.E. of $n \geq 36$ cells from three different experiments. Significant differences from the control are indicated by *asterisks* (*) ($p < 0.01$).

FIG. 6. **Targeted disruption of the *Aqp5* gene inhibits hypotonicity-induced cell swelling and the associated RVD sublingual acinar cells.** The role of AQP5 in the RVD response was examined in sublingual acinar cells loaded with calcein as described under "Experimental Procedures." *Panel A*, sublingual acini isolated from *Aqp5$^{+/+}$* (*solid line*) and *Aqp5$^{-/-}$* (*dotted line*) were perfused in an isosmotic solution, and then hyposomotic cell swelling was induced by switching the perfusate to a second medium diluted with 30% water during the time interval indicated by the *cross-hatched rectangle*. Changes in cell volume are represented as values of 1/F_n. *Panels B and C*, summaries of the relative rates of swelling (*panel B*) and RVD (*panel C*), respectively, in *Aqp5$^{+/+}$* (*filled bar*) and *Aqp5$^{-/-}$* (*open bar*) sublingual acinar cells. Values represent mean ± S.E. of $n \geq 36$ cells from three different experiments. Significant differences from the control are indicated by *asterisks* (*) ($p < 0.05$).

involved in acinar cell water permeability, the rate of volume change was determined in wild-type cells in response to a hypertonic stress in the presence and absence of HgCl$_2$. Water movement was osmotically driven by introducing a 30% hypertonic shock (see "Experimental Procedures"). Parotid (Fig. 3*A*) and sublingual (Fig. 4*A*) acinar cell volumes were measured by monitoring the fluorescence intensity of calcein within a defined intracellular volume, and the rate of cell shrinkage was used as an index of water permeability. The same cells were allowed to recover in isotonic medium prior to testing the Hg^{2+} sensitivity of the hypertonicity-induced changes in cell volume. The rate of hypertonicity-induced cell shrinkage was then determined in the presence of HgCl$_2$ after a 5-min preincubation in 1 mM HgCl$_2$. An approximate 50% decrease ($p < 0.0001$, $n \geq$ 36) in the rate of shrinkage was observed in the presence of HgCl$_2$ in wild-type parotid cells (Fig. 3*A*), and an ~35% decrease ($p < 0.0001$, n ≥ 36) was seen in wild-type sublingual acinar cells (Fig. 4*A*) in response to hypertonic challenge. The volume change resistant to inhibition by HgCl$_2$ represents the intrinsic water permeability of the plasma membrane as well as the water transport mediated by aquaporins not blocked by mercury.

As observed after inhibition with HgCl$_2$, knocking out the *Aqp5* gene dramatically reduced the water permeability of acinar cells. An ~65% decrease in the rate of hypertonicity-induced cell shrinkage was observed in *Aqp5$^{-/-}$* parotid acinar cells compared with wild-type acinar cells (Fig. 3*B*), and an

~77% decrease in the rate of cell shrinkage was observed in *Aqp5$^{-/-}$* sublingual acinar cells (Fig. 4*B*). These results indicate that AQP5 is involved in mediating the water permeability of acinar cells. Mercury did not inhibit water movement in *Aqp5$^{-/-}$* acinar cells but actually enhanced the water permeability of both parotid and sublingual *Aqp5$^{-/-}$* acinar cells by an unknown mechanism (Figs. 3*B* and 4*B*; $p < 0.0001$; $n \geq 36$).

Hyposomotic Cell Swelling and Associated RVD—Isolated parotid and sublingual acinar cells (Figs. 5 and 6, respectively) from *Aqp5$^{+/+}$* and *Aqp5$^{-/-}$* mice were subjected to a hyposmotic shock, and the rates of cell swelling and the subsequent RVD were monitored. Water permeability was significantly less in parotid (Fig. 5, *B* and *C*; $p < 0.005$; $n \geq 16$;) and sublingual (Fig. 6, *B* and *C*; $p < 0.005$; $n \geq 39$) acinar cells from *Aqp5$^{-/-}$* mice compared with wild-type littermates. The rate of parotid acinar cell swelling was decreased by ~70% in *Aqp5$^{-/-}$* cells (Fig. 5*B*), with an accompanying ~58% decrease in the rate of RVD (Fig. 5*C*). Sublingual acinar cell swelling decreased by ~77% in *Aqp5$^{-/-}$* cells (Fig. 6*B*), with a coordinate ~60% decrease in the RVD rate (Fig. 6*C*). These data suggest that the AQP5-mediated water permeability is a major component in the regulatory volume decrease response. Moreover, a significant difference in the rate of RVD intrinsic to parotid *versus* sublingual acinar cells was observed (Figs. 5*C* and 6*C*, respectively). The rate of RVD for wild-type parotid acinar cells was determined to be 1.07 ± 0.20 units/min and was 0.40 ± 0.03 units/min for sublingual acinar cells. As a result, parotid acini

regulate their cell volume subsequent to swelling ~2.7-fold faster than sublingual acini from wild-type mice. Because the water permeabilities of parotid and sublingual acini were comparable in response to anisosmotic challenges (see Figs. 5*B* and 6*B*), the differences in the rates of RVD were probably caused by differences in the membrane permeability of ions in these two cell types.

DISCUSSION

Defects in water channel protein expression and/or function have been implicated in the pathogenesis of inherited and acquired forms of diseases of fluid imbalance (23, 24). To understand the molecular mechanisms by which the aquaporins regulate water balance in mammals, targeted disruption of individual aquaporins in mice has been actively investigated (AQP1 (25), AQP3 (26), AQP4 (27), AQP5 (10)).

We used AQP5-deficient mice to dissect the mechanisms by which AQP5 functions in the regulation of acinar cell volume and in the stimulation of salivary secretion. Northern and Western analyses show that mice homozygous for the targeted allele produce no full-length AQP5 mRNA and are null for AQP5 protein, respectively. Phenotypically, *Aqp5*$^{-/-}$ mice are 10% smaller in body weight compared with wild-type littermates. Birth genotypic ratios were 1:2:0.5 and deviated from the expected 1:2:1 Mendelian ratio, suggesting a role for AQP5 in prenatal development. The ratios observed by us also differ from a previously published report by Ma *et al.* (10), indicating an observed 1 (*Aqp5*$^{+/+}$): 1 (*Aqp5*$^{+/-}$): 0.4 (*Aqp5*$^{-/-}$) ratio of F2 litters in an independently generated AQP5-deficient mouse strain. It is possible that the difference observed between our results (1 (*Aqp5*$^{+/+}$): 2 (*Aqp5*$^{+/-}$): 0.5 (*Aqp5*$^{-/-}$)) and the ratios reported by Ma *et al.* (10) is attributable to a difference in the genetic backgrounds of the two *Aqp5*-deficient strains.

Functionally, AQP5 deficiency results in dramatically reduced saliva production during pilocarpine stimulation. This result suggests two potential mechanisms whereby *Aqp5* disruption might induce hyposalivation. The simplest explanation is that AQP5 is required for transcellular water movement. Alternatively, targeted disruption of the *Aqp5* gene may alter whole animal water and electrolyte balance, resulting in a state of dehydration, a condition known to inhibit salivation (11, 12). To test this latter hypothesis, we measured multiple parameters related to whole animal water and electrolyte homeostasis. Loss of AQP5 function did not alter serum electrolyte and gas levels in AQP5 knockout mice. Likewise, urine osmolality and electrolyte composition, and urine output and water intake were not significantly different between wild-type and knockout mice, suggesting that AQP5 deficiency does not alter whole animal fluid homeostasis under normal physiological conditions.

Thus, decreased saliva production by mice lacking AQP5 cannot be explained easily by an indirect effect of water and electrolyte imbalance. This conclusion strongly suggests that the secretion defect observed in *Aqp5*$^{-/-}$ mice is caused by a loss of a critical transcellular water movement pathway. In fact, AQP5 deficiency results in a large decrease in mercury-sensitive, acinar cell water permeability as well as decreased ability of acinar cells to regulate cell volume under anisosmotic conditions. The regulation of acinar cell volume during salivary secretion is a dynamic process influenced by muscarinic and β-adrenergic stimulation, resulting in cell shrinkage and swelling, respectively. Mechanistically, changes in transepithelial osmotic forces drive fluid movement into the lumen and correlate with changes in acinar cell volume. Our data suggest that AQP5 is responsible for mediating the bulk of the acinar cell water permeability under anisosmotic conditions (≥65%). Interestingly, we observed that the addition of mercury to isolated *Aqp5*$^{-/-}$ parotid and sublingual acinar cells resulted in a relatively small but significant *increase* in water permeability. A recent study by Yasui *et al.* (30) reported a similar effect of mercury on the osmotic membrane permeability of oocytes expressing AQP6, a related water channel. It is therefore possible that an AQP6-like molecule is expressed in salivary gland acinar cells which is enhanced by the presence of mercury. It is also possible that mercury works nonspecifically to affect other membrane proteins, thereby affecting membrane permeability. Consistent with this latter possibility, mercury was also shown to mimic the effects of low pH on the activation of ion conductance in AQP6-expressing oocytes (30).

The *Aqp5* knockout mouse has also allowed us to evaluate the importance of this water channel in the context of whole animal physiology. The *in vivo* analysis of pilocarpine-stimulated salivary secretion and osmolality revealed that AQP5 is critically important in determining both saliva flow rates and final ionic composition. *Aqp5* null mice secrete saliva at an ~65% slower rate than wild-type mice, consistent with the ≥65% reduction of water permeability of acinar cells in the knockout mice (Fig. 2). In our studies, the average osmolality during the 15 min of saliva collection from wild-type mice was 171 mosm and 212 mosm during 2-mg and 10-mg pilocarpine stimulation, respectively. Our results are consistent with the observation that mammalian saliva, including that of the mouse saliva (29), is generally hypotonic (28). It is possible, but unlikely, that the difference in osmolality seen in our study and that reported by Ma *et al.* (10) is caused by the supramaximal concentration of pilocarpine used by Ma *et al.* (80 mg/kg of body weight), as our measurements of the average osmolality of the saliva collected from wild-type mice was 202 ± 2.6 mosm when 80 mg of pilocarpine was used (data not shown, n = 6). Thus we also performed experiments using lower concentrations of pilocarpine which are likely closer to the physiological range of agonist concentrations (see Table I). Genetic background differences may explain the variation we observed in the osmolality between our *Aqp5* knockout mice and the *Aqp5* strain examined by Ma and colleagues (420 mosm).

Taken together, the cell volume measurements and *in vivo* measurements of saliva flow rates and composition reveal the critical mechanism by which fluid secretion is accomplished in the salivary gland. The cell volume measurements directly show that AQP5 regulates salivary secretion by increasing the membrane water permeability of acinar cells and that AQP5 regulates the cell volume of individual acinar cells. To date, this is the first reported evidence that deficiency in a water channel dramatically affects the regulation of cell volume in a native tissue. Based on the significant effect of AQP5 ablation on fluid secretion in the salivary gland, it is likely that other members of the mammalian AQP family which are involved in secretory or absorption may also be involved in controlling cell volume. The AQP5-deficient mouse may thus prove to be a useful animal model to investigate pathophysiological mechanisms of salivary gland dysfunction in humans.

REFERENCES

1. Bivona, P. L. (1998) *N. Y. State Dent. J.* **64,** 46–52
2. Astor, F. C., Hanft, K. L., and Ciocon, J. O. (1999) *Ear Nose Throat J.* **78,** 476–479
3. Fox, P. C. (1998) *Ann. N. Y. Acad. Sci.* **842,** 132–137
4. Turner, R. J., Paulais, M., Manganel, M., Lee, S. I., Moran, A., and Melvin, J. E. (1993) *Crit. Rev. Oral Biol. Med.* **4,** 384–391
5. He, X., Tse, C.-M., Donowitz, M., Alper, S. L., Gabriel, S. E., and Baum, B. J.

Salivary Gland Hypofunction in Aqp5$^{-/-}$ Mice

(1997) *Pfluegers Arch.* **433,** 260–268

6. Foskett, J. K., and Melvin, J. E. (1989) *Science* **244,** 1582–1585
7. Foskett, J. K. (1990) *Am. J. Physiol.* **259,** C998–C1004
8. Steward, M. C., Seo, Y., Murakami, M., Seo, J. T., Larcombe-McDouall, J. B., and Case, R. M. (1998) *Eur. J. Morphol.* **36,** 103–106
9. Matsuzaki, T., Suzuki, T., Koyama, H., Tanaka, S., and Takata, K. (1999) *Cell Tissue Res.* **295,** 513–521
10. Ma, T., Song, Y., Gillespie, A., Carlson, E. J., Epstein, C. J., and Verkman, A. S. (1999) *J. Biol. Chem.* **274,** 20071–20074
11. Fischer, D., and Ship, J. A. (1997) *Special Care Dent.* **17,** 58–64
12. Silanikove, N., and Tadmor, A. (1989) *Am. J. Physiol.* **256,** R809–815
13. Krane, C. M., Towne, J. E., and Menon, A. G. (1999) *Mamm. Genome* **10,** 498–505
14. Schultheis, P. J., Clarke, L. L., Meneton, P., Harline, M., Boivin, G. P., Stemmermann, G., Duffy, J. J., Doetschman, T., Miller, M. L., and Shull, G. E. (1998) *J. Clin. Invest.* **101,** 1243–1253
15. Askew, G. R., Doetschman, T., and Lingrel, J. B. (1993) *Mol. Cell. Biol.* **13,** 4115–4124
16. Stewart, C. L. (1993) *Methods Enzymol.* **225,** 823–856
17. Evans, R. L., Bell, S. M., Schultheis, P. J., Shull, G. E., and Melvin, J. E. (1999) *J. Biol. Chem.* **274,** 29025–29030
18. Schreiber, R., Nitschke, R., Greger, R., and Kunzelmann, K. (1999) *J. Biol. Chem.* **270,** 1908–1912

19. Spicer, A., Miller, M. L., Andringa, A., Riddle, T. M., Duffy, J. J., Doetschman, T., and Shull, G. E. (2000) *J. Biol. Chem.* **275,** 21555–21565
20. Heymann, J. B., and Engel, A. (2000) *J. Mol. Biol.* **295,** 1039–1053
21. Jung, J. S., Preston, G. M., Smith, B. L., Guggino, W. B., and Agre, P. (1994) *J. Biol. Chem.* **269,** 14648–14654
22. Raina, S., Preston, G. M., Guggino, W. B., and Agre, P. (1995) *J. Biol. Chem.* **270,** 1908–1912
23. King, L. S., Yasui, M., and Agre, P. (2000) *Mol. Med. Today* **6,** 60–65
24. Lee, M. D., King, L. S., and Agre, P. (1997) *Medicine* (*Baltimore*) **76,** 141–156
25. Ma, T., Yang, B., Gillespie, A., Carlson, E. J., Epstein, C. J., and Verkman, A. S. (1998) *J. Biol. Chem.* **273,** 4296–4299
26. Ma, T., Song, Y., Yang, B., Gillespie, A., Carlson, E. J., Epstein, C. J., and Verkman, A. S. (2000) *Proc. Natl. Acad. Sci. U. S. A.* **97,** 4386–4391
27. Ma, T., Yang, B., Gillespie, A., Carlson, E. J., Epstein, C. J., and Verkman, A. S. (1997) *J. Clin. Invest.* **100,** 957–962
28. Cook, D. I., Van Lennep, E. W., Roberts, M. L., and Young, J. A. (1994) in *Physiology of the Gastrointestinal Tract* (Johnson, L. R., ed) 3rd Ed., pp. 1061–1117, Raven Press, New York
29. Evans, R. L., Park, K., Turner, R. J., Watson, G. E., Nguyen, H. V., Dennett, M. R., Hand, A. R., Flagella, M., Shull, G. E., and Melvin, J. E. (2000) *J. Biol. Chem.* **275,** 26720–26726
30. Yasui, M., Hazama, A., Kwon, T. H., Nielsen, S., Guggino, W. B., and Agre, P. (1999) *Nature* **402,** 184–187

Salivary Acinar Cells from Aquaporin 5-deficient Mice Have Decreased Membrane Water Permeability and Altered Cell Volume Regulation

Carissa M. Krane, James E. Melvin, Ha-Van Nguyen, Linda Richardson, Jennifer E. Towne, Thomas Doetschman and Anil G. Menon